Phase-field model study of the effect of interface anisotropy on the crystal morphological evolution of cubic metals

R.S. Qin[a]* and H.K.D.H. Bhadeshia[a, b]

a. Graduate Institute of Ferrous Technology, Pohang University of Science and Technology, San 31, Hyojia-Dong Nam Gu, Pohang 790-784, Republic of Korea

b. Department of Materials Science and Metallurgy, University of Cambridge, Pembroke Street, Cambridge CB2 3QZ, UK

Abstract

An expression is proposed for the anisotropy of interfacial energy of cubic metals, based on the symmetry of the crystal structure. The associated coefficients can be determined experimentally or assessed using computational methods. Calculations demonstrate an average relative error of <3% in comparison with the embedded-atom data for face-centred cubic metals. For body-centred-cubic metals, the errors are around 7% due to discrepancies at {332} and {433} planes. The coefficients for {100}, {110}, {111} and {210} planes are well-behaved and can be used to simulate the consequences of interfacial anisotropy. The results have been applied in three-dimensional phase-field modelling of the evolution of crystal shapes, and the outcomes have been compared favourably with equilibrium shapes expected from Wulff's theorem.

1. Introduction

———————————
*Corresponding author. Tel: +82 54 2794407; fax: +82 54 2794499.
Email address: rsqin@postech.ac.kr

Crystals are by their very nature anisotropic and interfaces between crystals similarly have energies and structures which are orientation dependent. Phase-field models used to simulate microstructural development have attempted to incorporate this interfacial anisotropy in a variety of ways. The free energy density for a heterogeneous system with contributions from the chemical free energy and interface energy is represented by:

$$g(\varphi, c, T) = g_0(\varphi, c, T) + \frac{1}{2}\varepsilon^2 |\nabla \varphi|^2 \tag{1}$$

where g is the system free energy density, g_0 is the chemical free energy density, φ is phase-field order parameter, c is solute concentration, T is temperature and ε is the gradient energy coefficient. Interfacial anisotropy is generally introduced by making ε orientation-dependent. For example, in the two-dimensional simulation of cubic crystals it is common to assume that [1]

$$\varepsilon = \bar{\varepsilon}\left[1 + \gamma_\varepsilon \cos(k_\varepsilon \theta)\right] \tag{2}$$

where $\bar{\varepsilon}$ is the mean value of ε, θ is the polar angular coordinate of the interface normal, and γ_ε and k_ε are anisotropy parameters. Eq. (2) has been modified into other formats to fulfil specific simulation targets [2, 3]. In three-dimensional phase-field models, the Cahn-Hoffman ξ vector theory has been applied to describe the interface anisotropy [4, 5]. A suggestion made by Karma and Rappel for cubic crystals is [6]

$$\varepsilon = \bar{\varepsilon}\left[1 + \gamma_\varepsilon \left(n_x^4 + n_y^4 + n_z^4\right)\right] \tag{3}$$

where n_x, n_y and n_z are Cartesian coordinates of the interface normal. More recently, Haxhimali *et al.* suggested the gradient energy coefficient takes the following format to represent interface anisotropy in the context of phase-fields [7]:

$$\varepsilon = \bar{\varepsilon}\left[1 + \varepsilon_1 K_1(\theta, \Phi) + \varepsilon_2 K_2(\theta, \Phi) + \cdots\right] \tag{4}$$

where θ and Φ represent the orientation of the interface in spherical coordinates, ε_1 and ε_2 are coefficients reflecting the extents of anisotropy, K_1 and K_2 are cubic harmonics that are combinations of standard spherical harmonics with cubic symmetry. The addition of the $\varepsilon_2 K_2$ term in Eq. (4) (*cf.* Eq. (3)) is after reviewing molecular dynamics simulations for dendrite growth which suggest that this gives a better representation of anisotropy [8].

The motivation for the present work was to develop a generic expression for interface anisotropy of cubic metals, to specify coefficients in the resulting expression and to validate the concept against existing knowledge of crystal growth.

2. Interface energy anisotropy

In a cubic system, the normal to a plane with Miller indices (hkl) plane is the direction [hkl]. The unit normal $\hat{n}$ has its Cartesian coordinates n_x, n_y and n_z. Fig. 1 illustrates how these can be represented in polar or spherical coordinates:

$$n_x = \sin\theta\cos\phi = \frac{h}{\sqrt{h^2 + k^2 + l^2}} \tag{5.1}$$

$$n_y = \sin\theta\sin\phi = \frac{k}{\sqrt{h^2 + k^2 + l^2}} \tag{5.2}$$
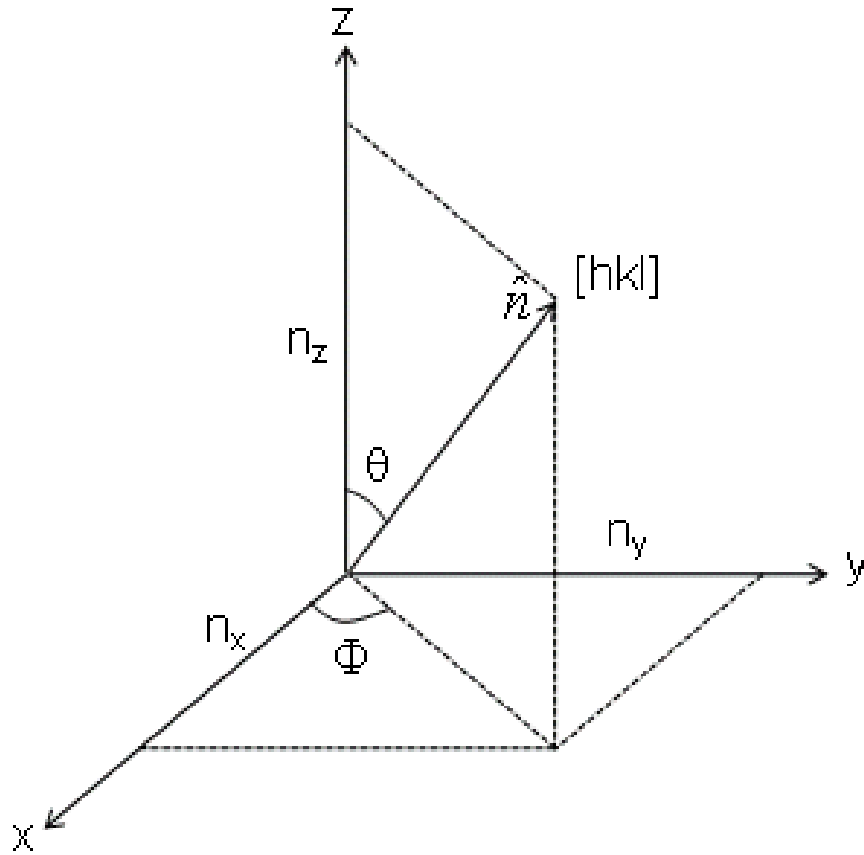
Fig. 1. Relation between Miller indices, Cartesian and polar coordinates in a cubic system.

$$n_z = \cos\theta = \frac{l}{\sqrt{h^2 + k^2 + l^2}} \tag{5.3}$$

Anisotropy energy, in general, can be represented as expansions of n_x, n_y and n_z in various orders. In discussing magnetocrystalline anisotropy [9], the interface anisotropy is represented by

$$\sigma(\hat{n}) = k_0 + \sum_{i,j} k_1 n_i n_j + \sum_{i,j,u,w} k_1 n_i n_j n_u n_w + \cdots \tag{6}$$

where k_0, k_1, k_2 and k_3 are the defining coefficients. The subscripts of n represent the Cartesian coordinates. For cubic symmetry, this simplifies into [10]

$$\sigma(\hat{n}) = k_0 + k_1 \left(n_x^2 n_y^2 + n_y^2 n_z^2 + n_z^2 n_x^2 \right) + k_2 n_x^2 n_y^2 n_z^2 + k_3 \left(n_x^2 n_y^2 + n_y^2 n_z^2 + n_z^2 n_x^2 \right)^2 + \cdots \tag{7}$$

Ignoring the higher order terms and using Miller indices, Eqs. (5) and (7) give

$$\sigma(h,k,l) = k_0 + k_1 \frac{h^2 k^2 + k^2 l^2 + l^2 h^2}{\left(h^2 + k^2 + l^2\right)^2} + k_2 \frac{h^2 k^2 l^2}{\left(h^2 + k^2 + l^2\right)^3} + k_3 \frac{\left(h^2 k^2 + k^2 l^2 + l^2 h^2\right)^2}{\left(h^2 + k^2 + l^2\right)^4} \tag{8}$$

For given anisotropy coefficients k_0, k_1, k_2 and k_3, Eq. (8) can express the interfacial energy as a function of orientation.

Eq.(8) is different from the expansion based on cubic harmonics [6, 7]. An example is that the leading anisotropic term in Eq.(7) is not $\left(n_x^4 + n_y^4 + n_z^4\right)$ but $\left(n_x^2 n_y^2 + n_y^2 n_z^2 + n_z^2 n_x^2\right)$. Critical assessment of those two different expressions for representing crystal anisotropy is important but is beyond the scope of the present work. However, it is obviously that Eq. (8) is consistent with cubic symmetry. For example, the interfacial energy for all directions of the form <100> is k_0. For <110> it is $k_0 + k_1 + k_3$, for <111> it is $k_0 + k_1/3 + k_2/9 + k_3/9$ etc. So in conclusion, although the individual coefficients cannot be identified with symmetry elements the equation as a whole is consistent with cubic symmetry.

It is required to validate the description inherent in Eq. (8) for cubic anisotropy. The method here was fitted to results from the embedded-atom method (EAM) [11, 12]. Those EAM calculations are based on embedding atomic functions and electronic densities given by Baskes et al. [13-15]. The least squares method was used to fit the data with the following objective function

$$\delta = \sum_i \left[\sigma(h,k,l) - \sigma_{EAM}(h,k,l)\right]^2 \tag{9}$$

where i is the total number of EAM data, $\sigma(h,k,l)$ is from Eq. (8) and $\sigma_{EAM}(h,k,l)$ from EAM data. The best values of k_0, k_1, k_2 and k_3 are obtained when δ achieves a minimum, i.e., at $\partial\delta / \partial k_j = 0$ with $j=0, 1, 2$ and 3. Fig. 2 demonstrates the efficacy of Eq. (8) for 10 face-centred cubic (fcc) crystals, and the corresponding derived values of anisotropy coefficients together with the average relative errors (AvRE) are listed in table 1. AvRE is defined as $AvRE = \overline{[|\sigma(h,k,l) - \sigma_{EAM}(h,k,l)| / \sigma_{EAM}(h,k,l)]}$. It can be seen that 9 out of ten fits have <2% average relative errors. In the case of aluminium, the error is $< 2.9\%$. This shows that Eq. 8 gives a good description of interface anisotropy in fcc crystals.
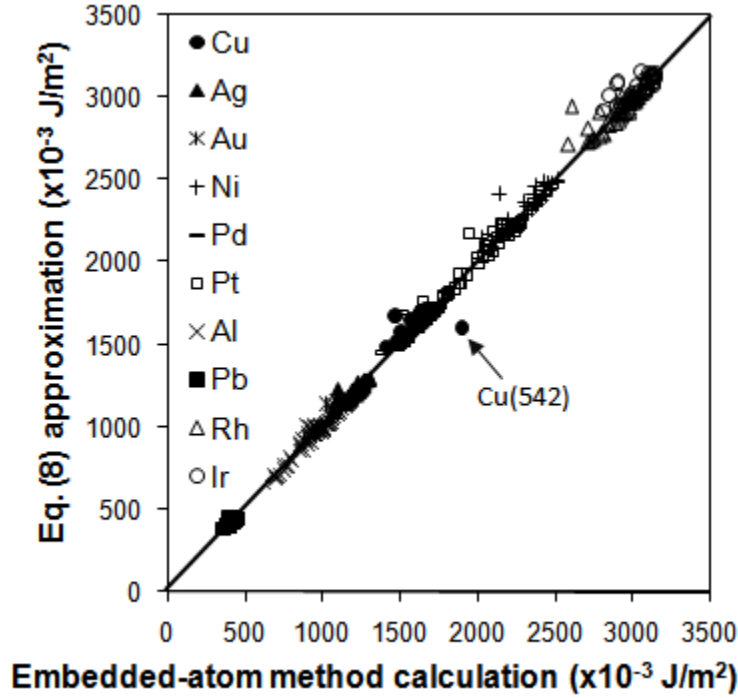
Fig. 2. Comparison of interface energy of face-centred cubic crystals calculated by Eq. (8) with data from the embedded-atom method.

Table 1 Anisotropy coefficients k_0, k_1, k_2, k_3 and AvRE determined by least squares fitting of EAM data. The units for coefficients are in erg/cm^2. AvRE4% is for the data plotted in Fig. 4.

Metal	k_0	k_1	k_2	k_3	AvRE (%)	AvRE4(%)
Cu	1666.87	733.621	-1873.19	-3260.43	1.959	2.802
Ag	1287.51	110.57	-642.8	-1401.67	1.527	2.369
Au	1101.41	917.506	-2658.9	-3358.65	1.850	2.586
Ni	2462.4	723.47	-2970.25	-4075.9	1.637	2.426
Pd	1685.19	975.872	-2015.65	-4055.37	1.782	2.478
Pt	2197.7	926.172	-6581.9	-4542.32	1.854	2.676
Al	922.344	1363.19	-5690.92	-4478.54	2.856	3.568
Pb	430.362	280.798	-493.042	-1082.85	1.614	2.463
Rh	2934.53	1495.79	-486.378	-6338.95	1.671	2.357
Ir	2943.61	2547.81	1421.33	-8266	1.445	2.179
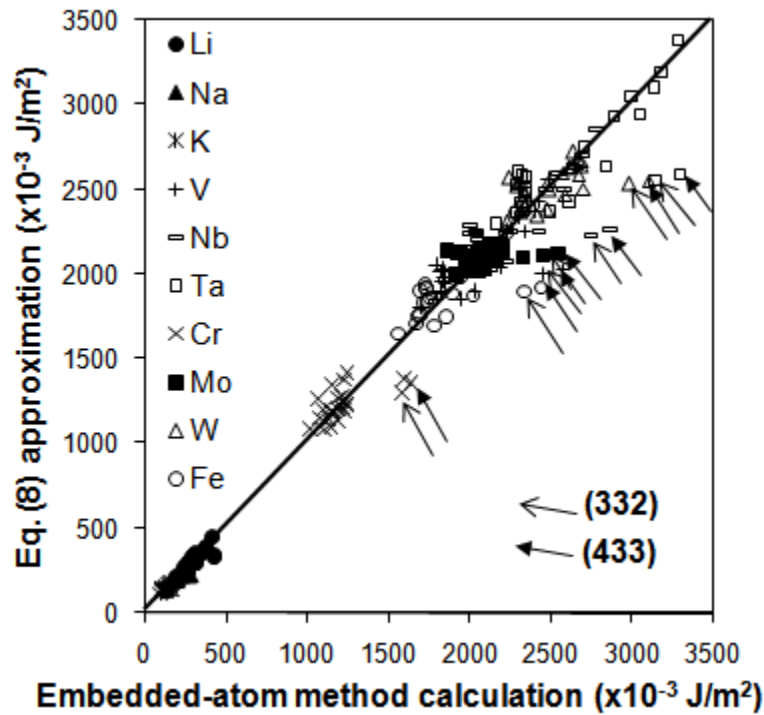
Fig. 3. Comparison of interface energy of body-centred cubic crystals calculated by Eq. (8) with numerical results from embedded-atom method.

The corresponding data for body-centred cubic crystals are in Fig. 3 and table 2, with most AvRE values at around 6%. Lithium has the largest AvRE at 8.7%. The discrepancies are

especially severe for the (332) and (433) planes for all the considered bcc metals. This suggests a potential problem with the EAM calculations and atomic potential and electronic densities for those two orientations. Without those two discrepancies, the fitness could be improved substantially.

Table 2 Anisotropy coefficients k_0, k_1, k_2, k_3 and AvRE determined by least squares fitting of EAM data. The units for coefficients are in erg/cm^2. AvRE4% is for the data plotted in Fig. 4.

Metal	k_0	k_1	k_2	k_3	AvRE (%)	AvRE4(%)
Li	442.723	-1163.95	4554.7	1123.37	8.713	9.640
Na	295.162	-578.775	1914.79	476.77	7.195	7.707
K	186.96	-347.872	1021.95	281.641	7.038	7.543
V	2561.47	-3584.81	11986.8	2134.02	6.059	6.100
Nb	2861.21	-4256.08	14414.2	2764.52	6.202	6.291
Ta	3381.3	-5271.41	15268.7	3735.67	6.367	6.596
Cr	1286.05	-1306.83	9485.12	1917.94	6.909	6.623
Mo	2184.48	-343.473	7098.62	-1783.23	5.202	4.660
W	2726.18	-1493.07	11203.9	-639.744	5.427	5.083
Fe	2258.53	-3291.47	12959.9	1880.74	6.069	6.052

It is worth pointing out that k_0 in tables 1 and 2 does not equal the averaged interface energy. However, this can be easily done by a stepped least squares method of using $\sigma(h,k,l) = k_0$ to fit data and determine k_0 first. Other parameters are determined subsequently. Despite the advantage that k_0 reproduces the average interface energy exactly, it is found that the stepped least square method gives less accuracy in data-fitting. Application of the stepped least squares method for Cu, Ag and Au result AeRV values of 4.043 %, 3.276% and 5.025%, respectively.

There are in Eq. (8) only four unknown coefficients which can be fully determined by calculating or measuring the interfacial energy at just four different orientations. Fig. 4 illustrates the comparison of all EAM calculations with the Eq. (8) where the anisotropy
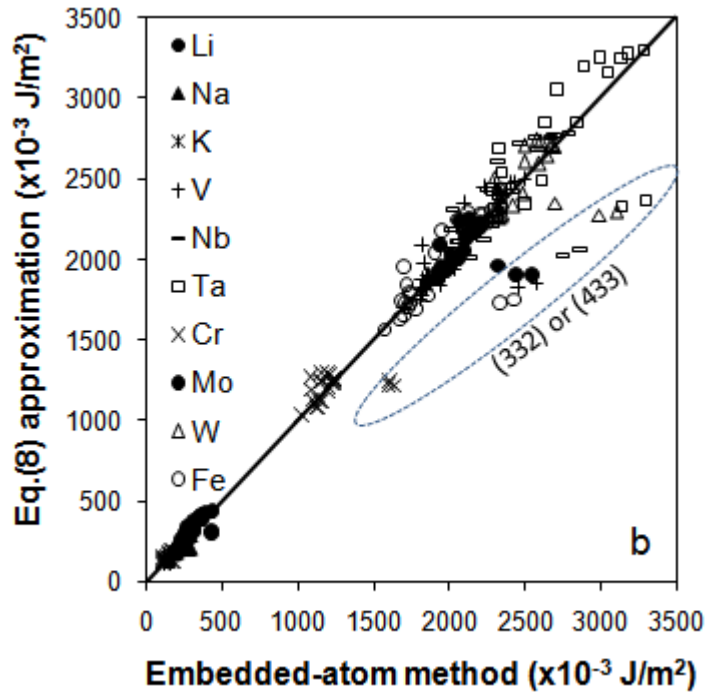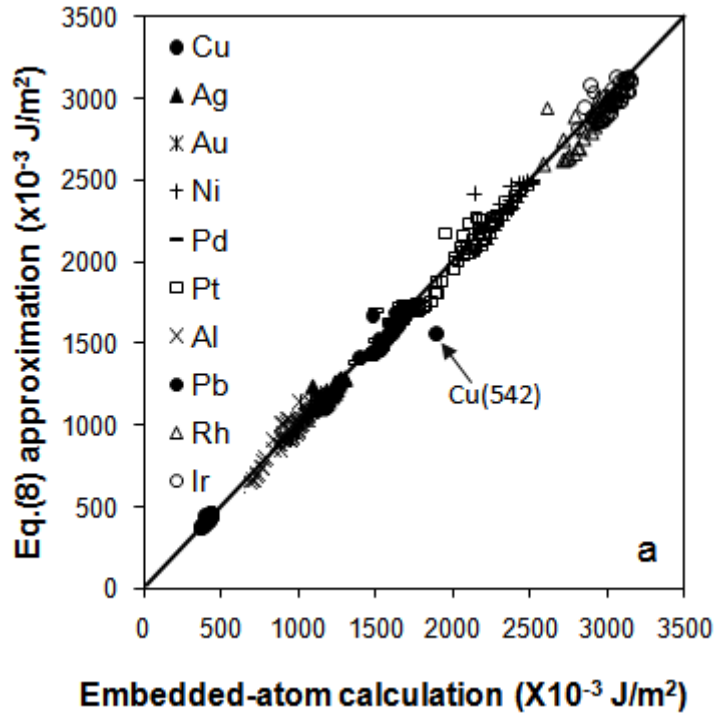
Fig. 4. Comparison of Eq. (8) calculation where coefficients are determined by (100), (110), (111) and (210) with all available EAM data. (a) fcc crystal; (b) bcc crystal.

coefficients k_0, k_1, k_2 and k_3 are determined by only using the interface energies at (100), (110), (111) and (210). The corresponding AvRE values regarding to this calculation are listed in table 1 and table 2 with column entitled AvRE4. All data show that AvRE4 is less than 1% larger than AvRE. AvRE4 values for Cr, Mo, W and Fe are even smaller than the corresponding AvRE values. It is seen that the accuracy of this computation is comparable to the large data-fitting illustrated in Figs. 2 and 3. This suggests that there is redundant information in the EAM calculations, so that such computations could be done more economically by focusing just on the solution of the four coefficients of Eq. 8, and hence on the study of just four interface orientations.

3. Phase-field model consideration

Eqs. (7) and (8) are for the interfacial energy per unit area, σ, which in a phase field model is implicitly represented by the gradient energy coefficient ε. We now consider the relationship between these two quantities in the context of the simplest phase-field model (Eq. 1). For the system in which phase transition takes place from $\varphi = 0$ to $\varphi = 1$, the chemical free energy density g_0 can be described by a double-well potential function [16, 17].

$$g_0(\varphi,c,T) = g_b(\varphi) + \frac{1}{4\omega}\varphi^2(1-\varphi)^2 \tag{10}$$

where g_b is the chemical free energy of $\varphi = 0$ and $\varphi = 1$ bulk phases, and ω is a coefficient reflecting the kinetic barrier between two minima. The governing equation for the evolution of the phase-field order parameter φ is [5]

$$\frac{\partial \varphi}{\partial t} = M_\phi \left(\nabla \frac{\partial g}{\partial \nabla \varphi} - \frac{\partial g}{\partial \varphi} \right) \tag{11}$$

where M_φ is the phase-field mobility and its value can be derived from interface kinetics [5, 18-19]. Inserting Eqs. (1) and (10) into (11) leads to [6]

$$\frac{\partial \varphi}{\partial t} = M_\varphi \left\{ \frac{\partial}{\partial x}\left[|\nabla \varphi|^2 \varepsilon(\hat{n}) \frac{\partial \varepsilon(\hat{n})}{\partial(\varphi_x)} \right] + \frac{\partial}{\partial y}\left[|\nabla \varphi|^2 \varepsilon(\hat{n}) \frac{\partial \varepsilon(\hat{n})}{\partial(\varphi_y)} \right] + \frac{\partial}{\partial z}\left[|\nabla \varphi|^2 \varepsilon(\hat{n}) \frac{\partial \varepsilon(\hat{n})}{\partial(\varphi_z)} \right] \right\}$$

$$+\nabla\left[\varepsilon(\hat{n})^2\nabla\varphi\right]-\frac{1}{2\omega}\varphi(1-\varphi)(1-2\varphi)-\frac{\partial g_b}{\partial\varphi}\right\} \tag{12}$$

In the one-dimensional system where the interface is constant along the axis, Eq. (12) is reduced at equilibrium to

$$\varepsilon^2\frac{d^2\varphi}{dx^2}-\frac{1}{2\omega}\varphi(1-\varphi)(1-2\varphi)=0 \tag{13}$$

The solution of the equation for the boundary conditions $\varphi = 1$ at $x = -\infty$ and $\varphi = 0$ at $x = +\infty$ is

$$\varphi(x)=\frac{1}{2}\left[1-\tanh\frac{x}{2\sqrt{2\omega\varepsilon}}\right] \tag{14}$$

Let

$$\lambda=2.2\sqrt{2\omega}\varepsilon \tag{15}$$

Eqs. (14) and (15) give $\varphi(-\lambda)=0.90025$ and $\varphi(-\lambda)=0.0975$, which is a good approximation of interface thickness. λ is called the half-interface thickness because the interface starts from $-\lambda$ and ends at λ. Multiplying Eq. (13) with $d\varphi/dx$ and integrating leads to

$$\frac{1}{2}\varepsilon^2\left(\frac{d\varphi}{dx}\right)^2=\frac{1}{4\omega}\varphi^2(1-\varphi)^2 \tag{16}$$

The interface energy is all the excess energy at the interfacial region, which is

$$\sigma=\int_{-\infty}^{+\infty}\left[\frac{1}{2}\varepsilon^2\left(\frac{d\varphi}{dx}\right)^2+\frac{1}{4\omega}\varphi^2(1-\varphi)^2\right]=\varepsilon^2\int_{-\infty}^{+\infty}\left(\frac{d\varphi}{dx}\right)^2 dx \tag{17}$$

Insulting Eq. (14) into Eq. (17) leads to

$$\sigma=\frac{\sqrt{2}\varepsilon}{12\sqrt{\omega}} \tag{18}$$

Eqs. (15) and (18) give

$$\sigma=\frac{1.1}{3\lambda}\varepsilon^2 \tag{19}$$

A similar derivation is found in reference [17]. However, it is emphasized here that Eq. (19) is not only valid for a particular orientation but for any direction. This requires more rigorous mathematical derivation. In the suggestion, one has

$$\sigma(\hat{n}) = \frac{1.1}{3\lambda}\varepsilon(\hat{n})^2 \tag{20}$$

Suppose the gradient energy coefficient has the following format

$$\varepsilon(\hat{n}) = \varepsilon_0 + \varepsilon_1\left(n_x^2 n_y^2 + n_y^2 n_z^2 + n_z^2 n_x^2\right) + \varepsilon_2 n_x^2 n_y^2 n_z^2 + \varepsilon_3\left(n_x^2 n_y^2 + n_y^2 n_z^2 + n_z^2 n_x^2\right)^2 \tag{21}$$

Bringing Eq. (21) into Eq. (20), ignoring the higher order terms and comparing the results with Eq. 7, it gives

$$\varepsilon_0 = \lambda_0 \sqrt{k_0} \tag{22.1}$$

$$\varepsilon_1 = \frac{\lambda_0 k_1}{2\sqrt{k_0}} \tag{22.2}$$

$$\varepsilon_2 = \frac{\lambda_0 k_2}{2\sqrt{k_0}} \tag{22.3}$$

$$\varepsilon_3 = \frac{\lambda_0 k_3}{2\sqrt{k_0}} - \frac{\lambda_0 k_1^2}{8k_0\sqrt{k_0}} \tag{22.4}$$

where $\lambda_0 = \sqrt{3\lambda/1.1}$. Eq. (22) fully determines the coefficients of gradient energy coefficient function in terms of the coefficients in the anisotropic interface energy function. The theory is now closed. Table 3 lists some of the results obtained from data given in table 1.

Table 3. Coefficients in gradient energy equation

Metal	$\varepsilon_1/\varepsilon_0$	$\varepsilon_2/\varepsilon_0$	$\varepsilon_3/\varepsilon_0$
Cu	0.22	-0.56	-1.00
Ag	0.04	-0.25	-0.55
Au	0.42	-1.21	-1.61
Ni	0.15	-0.60	-0.84
Pd	0.29	-0.60	-1.25
Pt	0.21	-1.50	-1.06
Al	0.74	-3.09	-2.70
Pb	0.33	-0.57	-1.31
Rh	0.25	-0.08	-1.11

Ir	0.43	0.24	-1.50

The interface normal vector in the phase-field model is computed by

$$\hat{n} = \frac{\nabla \varphi}{|\nabla \varphi|} \qquad (23)$$

This gives $n_j = \varphi_j / \sqrt{\sum_j \varphi_j^2}$, where j represents one of the axes in Cartesian coordinates

and $\varphi_j = \partial \varphi / \partial x_j$. Other basic terms in the further expansion of Eq. (12) include

$\partial n_j / \partial x_k = \varphi_{jk} / |\nabla \varphi| - \varphi_j \sum_m \varphi_m \varphi_{mk} / |\nabla \varphi|^3$, $\quad \partial n_j / \partial \varphi_k = \delta_{jk} / |\nabla \varphi| - \varphi_j \varphi_k / |\nabla \varphi|^3$ etc. The

computation of Eq. (12) also requires the definition of the format of $g_b(\varphi)$. In the

isothermal and composition-invariant phase-transitions, it can be represented as [6]

$$g_b(\varphi) = [1 - h(\varphi)]g_0 + h(\varphi)g_1 \qquad (24)$$

where g_0 and g_1 are free energy densities of the bulk phases $\varphi = 0$ and $\varphi = 1$, respectively.

$h(\varphi) = \varphi^2(6\varphi^2 - 15\varphi + 10)$ can be considered as the fraction of the phase $\varphi = 1$, so that

$$\frac{\partial g_b}{\partial \varphi} = 30\varphi^2(1 - \varphi)^2(g_0 - g_1) \qquad (25)$$

There are other suggestions for dealing with different systems [20, 21]. The phase-field

computation is solving Eq. (11) by discrete method under specified materials parameters.

4. Numerical computation and discussion

Phase-field computations were carried out for studying the effect of interface anisotropy on

crystal morphology evolution. For reducing other effects it is supposed that all the

parameters are fixed in the calculations except the interface anisotropy. Three sets of

parameters are applied, as listed in table 4. The polar diagrams of Eq. (21) with those three

sets of parameters are demonstrated in Fig. 5.
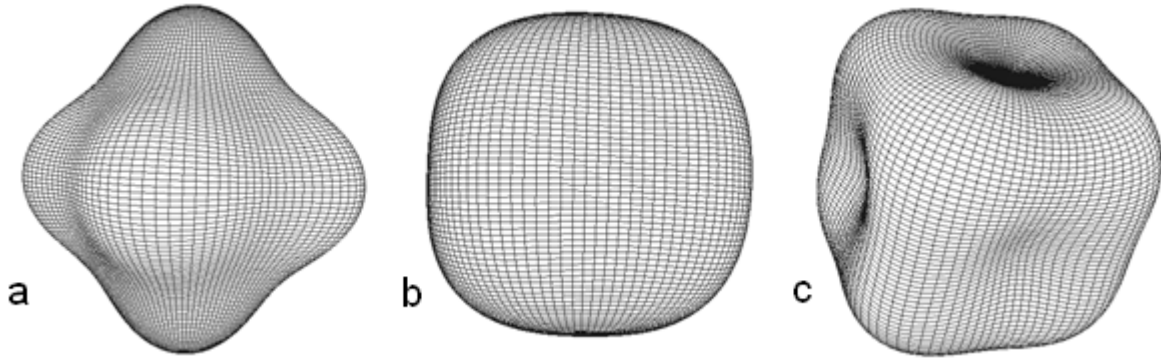
Fig.5. Polar diagram of Eq. (21) with various coefficients: (a) Case A, (b) Case B and (c) Case C.
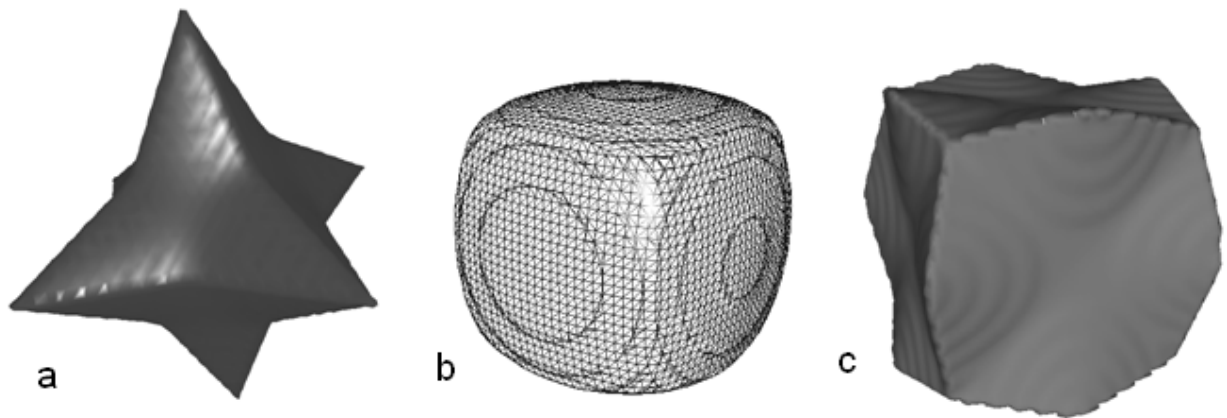
Fig.6. Crystal morphology at 5000 time steps as a function of interfacial anisotropy: (a) Case A, (b) Case B and (c) Case C.

Table 4. Coefficients applied in phase-field calculation

	Case A	Case B	Case C
$\varepsilon_1 / \varepsilon_0$	-0.863	0.402	1.8655
$\varepsilon_2 / \varepsilon_0$	0.395	0.00144	0.2555
$\varepsilon_3 / \varepsilon_0$	0.0238	0.00066	0.0

It is chosen that $g_0 - g_1 = 3.6 \times 10^8 \, J/m^3$, $k_0 = 0.8 \, J/m^2$, $M_\varphi = 100$ and $\lambda = 14.3$ nm in

the simulations. k_0 and λ give $\omega = 1.3547 \times 10^{-9} \, m^3/J$ and $\varepsilon_0 = 2.488 \times 10^{-4} \, J^{\frac{1}{2}}/m^{\frac{1}{2}}$. Eq.

(12) is solved by a 6-neighbour implicit finite difference method at three dimensional

uniform 128^3 grids. The grid size is chosen as $\Delta x=0.5\lambda$ so that interface covers 4 elements

[20, 22]. The initial condition is to put a spherical seed at the centre of the logistic frame

with the phase-field order parameter configured to

$$\begin{cases} \varphi(r,t=0)=1 & \text{for} \quad r < \Delta x \\ \varphi(r,t=0)=\dfrac{2}{1+\exp(r-1)} & \text{for} \quad \Delta x < r < 4\Delta x \\ \varphi(r,t=0)=0 & \text{for} \quad r \geq 4\Delta x \end{cases} \qquad (26)$$

The crystal morphologies at 5000 time steps for all three different interface anisotropy

cases are demonstrated in Fig. 6. It can be seen clearly that the crystal morphologies are

completely different for different interface anisotropy even when all other parameters are

fixed. In other words, interfacial anisotropy can have an important impact on crystal

morphological evolution.

In the phase-field simulation of crystal growth, $\partial g_b / \partial \varphi$ plays the role of driving force for

the phase transition. The phase-field simulation in the current work assumes a constant

$(g_0 - g_1)$ without consideration of thermal and solute diffusion. This means that there is no

equilibrium mechanism for the growing crystals to approach their equilibrium shape. It is

observed, as is expected for the earlier consideration, that the shapes of crystals at different

time steps are similar. The interface thickness maintains the 4-grid-distance value all way

through the growth.

Although the crystal shapes obtained in the current work are not equilibrium, it is

interesting to compare the non-equilibrium crystal shapes with the equilibrium ones. The

equilibrium shape of crystal, according to Wulff's theorem, takes the inner envelope of the

polar interface energy diagram so that the crystal interface energy for a given volume is

minimized [23]. Fig. 7 shows the polar interface energy diagram, phase-field model

simulated non-equilibrium crystal shape, and the equilibrium crystal shape predicted by

Wulff's theorem, for the three sets of anisotropic parameters listed in table 4. It is found that the non-equilibrium crystal shapes, especially the growing crystal tips, possess some favorable correlations with the equilibrium crystal shape. For example, Figs. 7(a) and 7(c) show the sharp crystal tip but Fig. 7(b) shows round corners. The evolution of crystal geometry from the non-equilibrium to equilibrium has been studied by phase-field modelling as well as other methods [24, 25].

It is worth pointing out that although phase-field simulation can sometimes produce a crystal shape which is the same as that of the equilibrium shape predicted by Wulff's theorem, the crystal is not at equilibrium. Equilibrium shape must correspond to an equilibrium state. For example, choosing $(g_0 - g_1) = 1.358 \times 10^9$ J/m^3 and retaining all the other parameters the same as the early definition, the Case A anisotropy will lead to missing orientations and cusps, which is exactly the equilibrium shape illustrated in Fig. 7(a) but is non-equilibrium crystal.

polar diagram of
interface energy

equilibrium crystal boundary
predicted by Wulff's theory

non-equilibrium crystal boundary
by phase-field simulation

b

polar diagram of
interface energy

non-equilibrium crystal
boundary by phase-field
simulation

equilibrium crystal boundary
predicted by Wulff's theory

c
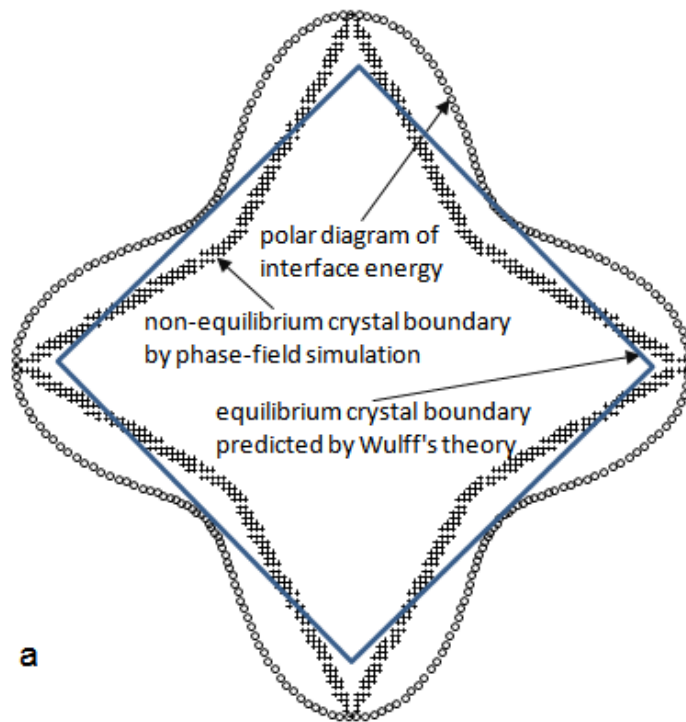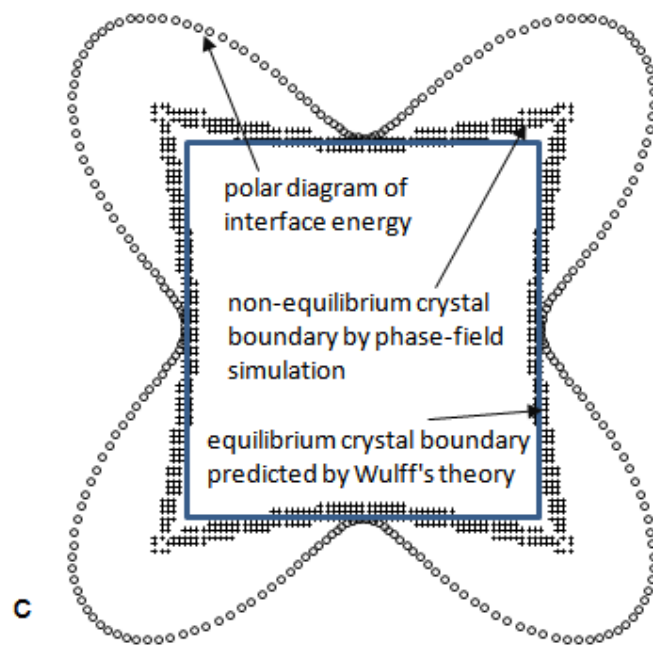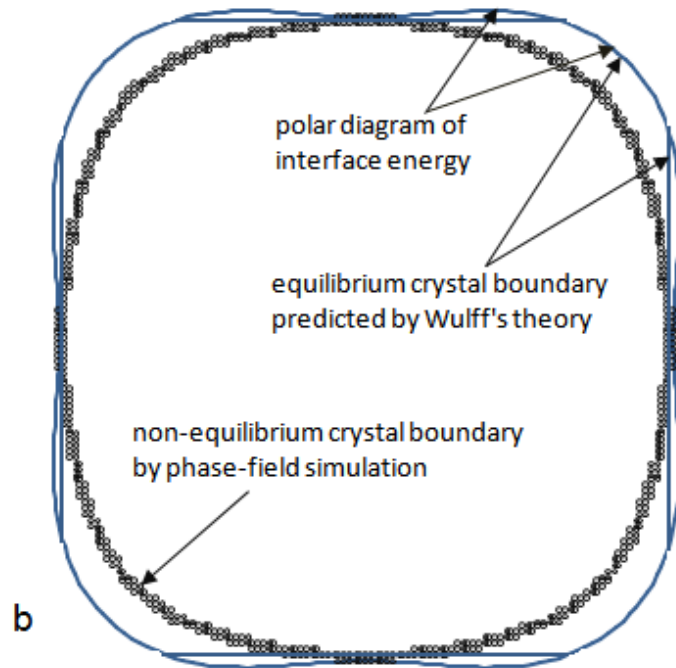
Fig. 7. Two-dimensional sections of three-dimensional polar diagrams of interface energy, equilibrium crystal shape predicted by Wulff's theorem, and phase-field simulated non-

equilibrium crystal shape in X-Y plane where $\theta = \pi/2$ with interface anisotropy parameters defined by (a) Case A, (B) Case B and (C) Case C.

5. Conclusions

(1) Anisotropic interface energy of cubic crystals is analyzed and is suggested to be represented as $\sigma(\hat{n}) = k_0 + k_1\left(n_x^2 n_y^2 + n_y^2 n_z^2 + n_z^2 n_x^2\right) + k_2 n_x^2 n_y^2 n_z^2$ $+ k_3\left(n_x^2 n_y^2 + n_y^2 n_z^2 + n_z^2 n_x^2\right)^2$. Using Miller indices it is represented as

$$\sigma(h,k,l) = k_0 + k_1 \frac{h^2 k^2 + k^2 l^2 + l^2 h^2}{\left(h^2 + k^2 + l^2\right)^2} + k_2 \frac{h^2 k^2 l^2}{\left(h^2 + k^2 + l^2\right)^3} + k_3 \frac{\left(h^2 k^2 + k^2 l^2 + l^2 h^2\right)^2}{\left(h^2 + k^2 + l^2\right)^4}$$

. The coefficients of k_0, k_1, k_2 and k_3 can be determined by experimental measurements or atomistic computations. The fitting of data obtained by embedded-atom method calculations of face-centred cubic and body-centred cubic metals show the good agreement. This proves that the suggested expression is reasonable.

(2) The parameters k_0, k_1, k_2 and k_3 that are specified by just the interface energies at (100), (110), (111) and (210) give good predictions of other orientations of planes. This suggests that fewer measurement or computations are required in the determination of interface anisotropy.

(3) The gradient energy coefficient in phase-field model should take the format $\varepsilon(\hat{n}) = \varepsilon_0 + \varepsilon_1\left(n_x^2 n_y^2 + n_y^2 n_z^2 + n_z^2 n_x^2\right) + \varepsilon_2 n_x^2 n_y^2 n_z^2 + \varepsilon_3\left(n_x^2 n_y^2 + n_y^2 n_z^2 + n_z^2 n_x^2\right)^2$ where the coefficients can be determined by $\varepsilon_0 = \lambda_0\sqrt{k_0}$, $\varepsilon_1 = \dfrac{\lambda_0 k_1}{2\sqrt{k_0}}$, $\varepsilon_2 = \dfrac{\lambda_0 k_2}{2\sqrt{k_0}}$ and

$$\varepsilon_3 = \frac{\lambda_0 k_3}{2\sqrt{k_0}} - \frac{\lambda_0 k_1^2}{8k_0\sqrt{k_0}}.$$

(4) Phase-field simulations show that the interface anisotropy has a considerable impact on crystal morphological evolution. Just a small change of interface anisotropy while keeping all the other parameters unchanged, causes the crystal to grow into completely different shape.

(5) The effect of interface anisotropy on the equilibrium shape of crystal is determined by Wulff's theorem. The non-equilibrium crystal shape can have some important characteristics when comparing with its equilibrium shape.

Acknowledgements

References

[1] Wheeler AA, Murray BT. Physica D 1993;66:243.

[2] Moelans N, Blanpain B, Wollants P. Phys Rev Lett 2008; 101:025502.

[3] Loginova I, Ågren J, Amberg G. Acta Mater. 2004; 52:4055.

[4] Wheeler AA, McFadden GB. Proc R Soc London A 1997;453:1611.

[5] Nestler B, Wheeler AA. Phys Rev E 1998; 57:2602.

[6] Karma A, Rappel WJ. Phys Rev E 1998; 57:4323.

[7] Haxhimali T, Karma A, Gonzales F, Rappaz M. Nature Mater. 2006; 5:660.

[8] Hoyt JJ, Asta M, Karma A. Mater Sci Eng. R 2003; 41:121–163.

[9] Braun A. Physica B 2006; 373:346.

[10] Braun A, Feldmann B, Wuttig M. J Magn Magn Mater. 1997;171:16.

[11] Zhang JM, Ma F, Xu KW. Appl Surf Sci. 2004; 229:34.

[12] Zhang JM, Ma F, Xu KW. Surf Interface Anal. 2003; 35:662.

[13] Baskes MI. Phys Rev Lett. 1987; 59:2666.

[14] Baskes MI, Nelson JS, Wright AF. Phys Rev B 1989; 40:6086.

[15] Baskes MI. Phys Rev B 1992; 46:2727.

[16] Wheeler AA, Boettinger WJ, McFadden GB. Phys Rev A 1992; 45:7424.

[17] Kim SG, Kim WT, Suzuki T. Phys Rev E 1998; 58:3316.

[18] Qin RS, Wallach ER. J Crys Growth 2003; 253:549.

[19] Qin RS, Wallach ER. Acta Mater. 2003; 51:6199.

[20] Qin RS, Wallach ER, Thomson RC. J Crys Growth 2005; 279:163.

[21] Chen LQ, Yang W. Phys Rev B 1994; 50:15752.

[22] Warren JA, Boettinger WJ. Acta Metall Mater. 1995;43:689.

[23] Wulff G. Z Kristallogr 1901;34:449.

[24] Eggleston JJ, McFadden GB, Voorhees, PW. Physica D 2001;150:91.

[25] Zhang W. J Crys Growth 2006; 297:169.